CME — EXPERIMENTAL RESULTS AND INTERPRETATION*

Fuqiang Wang

Purdue University, West Lafayette, Indiana 47907, USA
and
Huzhou University, Huzhou, Zhejiang 313000, China

Received 22 July 2022, accepted 21 September 2022, published online 14 December 2022

The experimental status is reviewed on the search for the chiral magnetic effect (CME) in relativistic heavy-ion collisions. Emphasis is put on background contributions to the CME-sensitive charge correlation measurements and their effects on data interpretation.

DOI:10.5506/APhysPolBSupp.16.1-A15

1. Introduction

The vacuum in quantum chromodynamics (QCD) possesses a property of the gluon field characterized by the Chern–Simons winding number or the topological charge (ΔQ). Interactions with $\Delta Q \neq 0$ gluon field would cause an imbalance in the (anti-)quark chirality. Such an imbalance can lead to charge separation along the direction of a strong magnetic field, a phenomenon called the chiral magnetic effect (CME) [1, 2]. It is theorized that the CME can arise in non-central heavy-ion collisions, where vacuum fluctuations to $\Delta Q \neq 0$ states are possible and where a strong transient magnetic field is present [3], while quantitative predictions are difficult [4, 5]. Since $\Delta Q \neq 0$ explicitly breaks the $\mathcal{CP}$ symmetry, an observation of the CME would not only verify a fundamental property of qcd but may also provide a natural solution to the matter–antimatter asymmetry of our universe.

The magnetic field created in heavy-ion collisions is on average perpendicular to the reaction plane (RP) [6]. A distinct signature of the CME is back-to-back emissions of opposite-sign (OS) charged hadrons and collimated emissions of the same-sign (SS) ones. This motivates the widely used observable, $\Delta\gamma \equiv \gamma_{\rm OS} - \gamma_{\rm SS}$, the difference in $\gamma_{\alpha\beta} = \langle\cos(\phi_\alpha + \phi_\beta - 2\Psi_{\rm RP})\rangle$ between OS and SS pairs (where ϕ_α and ϕ_β are their azimuthal angles and $\Psi_{\rm RP}$ is that of the RP) [7]. Several other observables [8, 9] have been proposed; since they are connected to $\Delta\gamma$ [10], only $\Delta\gamma$ will be reviewed here.

* Presented at the 29th International Conference on Ultrarelativistic Nucleus–Nucleus Collisions: Quark Matter 2022, Kraków, Poland, 4–10 April, 2022.

1.1. *Early measurements*

Figure 1 shows the first measurements of $\gamma_{\rm OS}$ and $\gamma_{\rm SS}$ at RHIC by STAR [11–13] and at the LHC by ALICE [14]. Large $\Delta\gamma$ signals were observed, qualitatively consistent with expectations from the CME. Although charge-independent backgrounds have canceled in $\Delta\gamma$, charge-dependent backgrounds remain [7, 15–17]. The larger $\Delta\gamma$ in Cu+Cu than Au+Au collisions is consistent with such backgrounds which are typically inversely proportional to multiplicity (N). It was warned in the first publications [11, 12] that *"[i]mproved theoretical calculations of the expected signal and potential physics backgrounds … are essential to understand whether or not the observed signal is due to [CME]"*

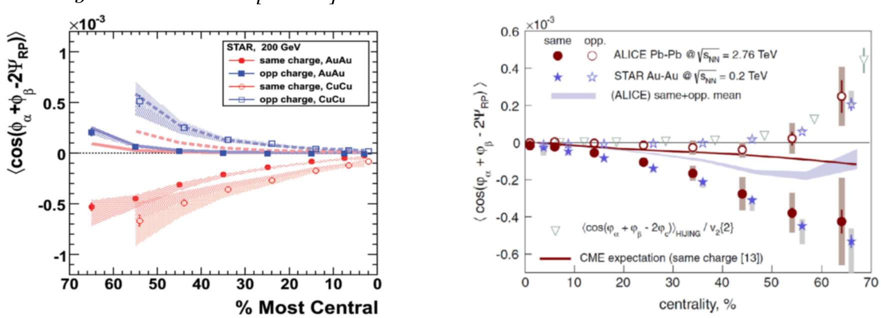

Fig. 1. First measurements of $\gamma_{\rm OS}$ and $\gamma_{\rm SS}$ in Au+Au and Cu+Cu collisions by RHIC/STAR [11, 12] (left) and in Pb+Pb collisions by LHC/ALICE [14] (right).

1.2. *Backgrounds*

The $\Delta\gamma$ is ambiguous between a back-to-back OS pair perpendicular to the RP (CME signal) and a collimated one parallel to it (background). Due to the elliptic flow (v_2), there are more resonances (or generally clusters) thus more OS pairs along the RP, leading to a background. It arises from the coupling of v_2 and genuine two-particle (2p) correlations (part of nonflow) [7, 18]

$$\Delta\gamma_{\rm Bkg} = N_{\rm cluster}/(N_\alpha N_\beta)\,\langle\cos(\phi_\alpha+\phi_\beta-2\phi_{\rm cluster})\rangle\, v_{2,\rm cluster}\,. \qquad (1)$$

Order of magnitude estimate suggests a background level of $0.2/100\times0.5\times0.1\sim10^{-4}$, comparable to the measured $\Delta\gamma$. In fact, the thermal and Blast-wave model parameterizations of particle yields and spectra data can reproduce the majority, if not the full, strength of the measurement [17, 19].

The first experimental indication that the background is large is the CMS measurement [20] in p+Pb collisions being comparable to that in Pb+Pb, as shown in Fig. 2 (left). A similar observation is made in p/d+Au collisions at RHIC [21]. In those small system collisions, the reconstructed event plane

(EP) is not correlated to the magnetic field direction, hence any CME would not be observable [20, 22]. Those small-system data suggest that the background can be large and, although the physics nature of backgrounds may differ, the $\Delta\gamma$ in heavy-ion collisions are likely dominated by backgrounds.

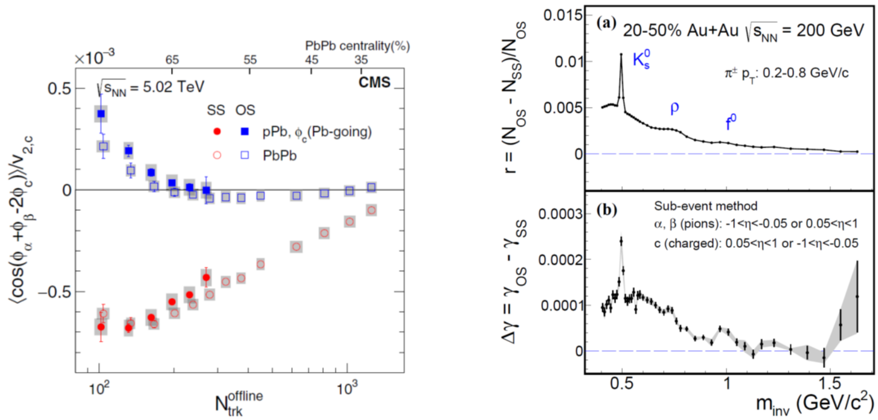

Fig. 2. (Left) The $\gamma_{\rm OS}$ and $\gamma_{\rm SS}$ in p+Pb and Pb+Pb collisions by the CMS [20]. (Right) The pair excess r and $\Delta\gamma$ *vs.* $m_{\rm inv}$ in Au+Au collisions by STAR [23].

An explicit demonstration of "resonance" background is the measurement of $\Delta\gamma$ as a function of the pair-invariant mass ($m_{\rm inv}$) [23]. This is shown in Fig. 2 (right), where the $\Delta\gamma$ is found to trace the OS over SS pair excess $r \equiv (N_{\rm OS} - N_{\rm SS})/N_{\rm OS}$, large at resonance masses on a continuum.

2. Early attempts to address backgrounds

There is no question that the background is large. The question is: How large is the background quantitatively? This question has to be answered experimentally when the background is large. Many attempts have been made to address the background issue [18, 24].

STAR has measured $\gamma_{\rm OS}$ and $\gamma_{\rm SS}$ in lower-energy Au+Au collisions at $\sqrt{s_{NN}}$ = 7.7–62.4 GeV [25], and the $\Delta\gamma$ is found to decrease toward lower energies. Inspired by $\Delta\gamma_{112} \equiv \Delta\gamma \approx \langle\cos(\phi_\alpha - \phi_\beta)\rangle\langle\cos 2(\phi_\beta - 2\Psi_2)\rangle \approx \kappa_2\Delta\delta v_2$ where $\Delta\delta \equiv \langle\cos(\phi_\alpha - \phi_\beta)\rangle$ [26], background estimate using the κ_2 parameter was attempted. However, the above trigonometry factorization is generally invalid (due to the ϕ_β in both factors) — otherwise the κ_2 should be unity. The correct factorization is given by Eq. (1). Because the κ_2 parameter is uncontrolled, rigorous conclusions cannot be drawn on CME.

It was suggested [19, 27] that $\kappa_3 \equiv \Delta\gamma_{123}/(\Delta\delta v_3)$, where $\Delta\gamma_{123}$ is the OS–SS difference of $\langle\cos(\phi_\alpha + 2\phi_\beta - 3\Psi_3)\rangle$, may be a good estimator of the background since no CME exists w.r.t. the third-order harmonic plane Ψ_3.

The κ_2 and κ_3 were indeed measured to be similar. However, from a $\Delta\gamma_{123}$ factorization similar to Eq. (1), it is clear that the backgrounds κ_3 and κ_2 do not equal. It is thus uncertain how to estimate CME background by κ_3.

Since $\Delta\gamma_{\rm Bkg} \propto v_2$, it is attempting to engineer on event shape (ESE) with vanishing v_2. This was first attempted by STAR [28] where the N-asymmetry correlation (a quantity similar to $\Delta\gamma$) is plotted against the observed $v_2^{\rm obs} = \langle\cos(\phi_{\rm POI} - \Psi_{\rm EP})\rangle$ of particles of interest (POI) in one half of the detector w.r.t. the EP from the other half. A similar technique has been recently proposed [29]. A linear relationship is observed as shown in Fig. 3 left panel; the $v_2^{\rm obs}$ can be negative because this ESE method engineers primarily on statistical fluctuations of v_2. The intercept at $v_2^{\rm obs} = 0$, consistent with zero in Fig. 3, would be more sensitive to CME. However, it has been found that residual background remains because resonance/cluster v_2, primarily responsible for the CME background, does not vanish at $v_2^{\rm obs} = 0$, as shown by the model study in Fig. 3 right panel [30].

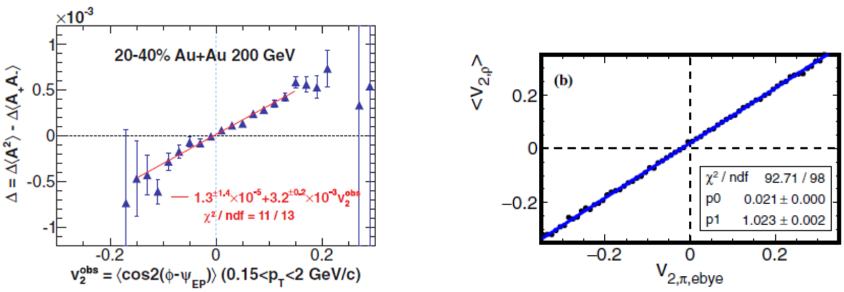

Fig. 3. STAR ESE analysis [28] engineering on statistical fluctuations of v_2 (left), and toy model study [30] of average v_2 of the ρ resonance vs. event-by-event pion v_2 in the final state (right).

ALICE [31] and CMS [27] have performed the ESE analysis by binning events according to the q_2 flow vector in the forward/backward region and then studying $\Delta\gamma$ as a function of the average v_2 of POI in those events in each centrality bin [32]. Linear relationships were observed. While analysis details differ, both experiments found vanishing intercepts at $v_2 = 0$, suggesting null CME signals. This method engineers on dynamical fluctuations of v_2, and remains a promising means to extract the possible CME, with nonflow effects to be assessed.

3. Latest measurements

Since the background is dominant, in order to extract the possible small CME signal, a delicate "cancellation" of background would be required, for which experiments often resort to comparative measures. Two such comparative measures have been carried out recently: one is isobar collisions and the other is correlations w.r.t. spectator plane SP) and participant plane (PP).

3.1. Isobar collisions

Isobar collisions were proposed [33, 34] as an ideal means to cancel the background: the same mass number of $^{96}_{44}$Ru and $^{96}_{40}$Zr would ensure the same background, and the larger atomic number in the former would yield a ∼15% stronger CME signal. This is supported by model calculations even including nuclear deformations [35]. If the CME is 10% of the measured $\Delta\gamma$, then an isobar difference of 1.5% would be expected, representing a 4σ effect with the precision of 0.4% achieved in experiment [36]. However, because $\Delta\gamma_{\rm Bkg} \propto 1/N$ and the magnetic field is smaller in isobar collisions than in Au+Au, the signal-to-background ratio in the former may be significantly smaller [37], which would result in a weaker significance.

Moreover, it has been shown by thedensity functional theory (DFT) calculations that the isobar nuclear structures are not identical — even though the charge radius of Ru is bigger, Zr possesses a significantly thicker neutron skin leading to its larger overall size [38, 39]. This would yield larger N and v_2 in Ru+Ru than Zr+Zr collisions at the same centrality. As a result, the backgrounds would be slightly different, with an uncertainty that may not be negligible, reducing the significance of isobar collisions [38]. Indeed, the isobar data show significant differences in N and v_2 between the two systems [36], consistent with dft predictions [38, 40].

Figure 4 shows the Ru+Ru/Zr+Zr ratio of various CME observables from STAR [36, 41, 42]. The ratio in $\Delta\gamma/v_2$ being significantly below unity is due to the N difference. The proper baseline would be the ratio in $1/N$, or unity for the ratio in $N\Delta\gamma/v_2$, the brown (lowest) dashed line in Fig. 4. The $\Delta\gamma$ data points are all above this line. This, however, cannot lead to the conclusion of a finite CME signal because of nonflow effects [43].

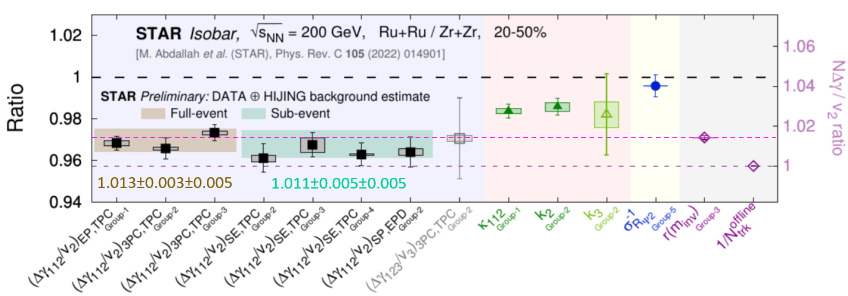

Fig. 4. (Color online) The Ru+Ru/Zr+Zr ratios of various CME observables by STAR [36, 42].

The nonflow effects have two parts [43]. One is simply because the measured v_2 contains nonflow (denoted as v_2^* henceforth, whereas those without asterisk now refer to the true flow), so it is propagated via $N\Delta\gamma/v_2^* \equiv$

NC_3/v_2^{*2} (similarly in the EP method). The other is a genuine 3-particle ($3p$) correlations, the last term in $C_3 \equiv \langle\cos(\phi_\alpha+\phi_\beta-2\phi_c)\rangle = \frac{C_{2p}N_{2p}}{N^2}v_{2,2p}v_2+\frac{C_{3p}N_{3p}}{2N^3}$, where $N \approx N_+ \approx N_-$ is POI multiplicities, $C_{2p} = \langle\cos(\phi_\alpha + \phi_\beta - 2\phi_{2p})\rangle$ and $C_{3p} = \langle\cos(\phi_\alpha + \phi_\beta - 2\phi_c)\rangle_{3p}$. Writing $v_2^{*2} = v_2^2 + v_{2,\mathrm{nf}}^2$ (where $v_{2,\mathrm{nf}}^2$ is nonflow contribution), and using shorthand notations $\epsilon_{\mathrm{nf}} \equiv v_{2,\mathrm{nf}}^2/v_2^2$, $\epsilon_2 \equiv \frac{C_{2p}N_{2p}}{N}\cdot\frac{v_{2,2p}}{v_2}$ and $\epsilon_3 \equiv \frac{C_{3p}N_{3p}}{2N}$, we have

$$\frac{\left(N\frac{\Delta\gamma}{v_2^*}\right)^{\mathrm{Ru}}}{\left(N\frac{\Delta\gamma}{v_2^*}\right)^{\mathrm{Zr}}} \approx \frac{\epsilon_2^{\mathrm{Ru}}}{\epsilon_2^{\mathrm{Zr}}} - \frac{\Delta\epsilon_{\mathrm{nf}}}{1+\epsilon_{\mathrm{nf}}} + \frac{\frac{\epsilon_3/\epsilon_2}{Nv_2^2}}{1+\frac{\epsilon_3/\epsilon_2}{Nv_2^2}}\left(\frac{\Delta\epsilon_3}{\epsilon_3} - \frac{\Delta\epsilon_2}{\epsilon_2} - \frac{\Delta N}{N} - \frac{\Delta v_2^2}{v_2^2}\right). \quad (2)$$

Here, $\Delta X \equiv X^{\mathrm{Ru}} - X^{\mathrm{Zr}}$, and variables without superscript refer to those in individual systems $X \approx X^{\mathrm{Ru}} \approx X^{\mathrm{Zr}}$. The first term in Eq. (2) r.h.s. characterizes deviation from N scaling — the background scales with N_{2p}/N^2 rather than simply $1/N$. This implies that the baseline should be the ratio of r, the pink (middle) dashed line in Fig. 4 [36]. The nonflow ϵ_{nf} can be assessed by $(\Delta\eta, \Delta\phi)$ $2p$ correlations. Preliminary data indicate a good cancellation between the effect of v_2 nonflow in the second term (positive, because $\Delta\epsilon_{\mathrm{nf}} < 0$ due to the larger N in Ru+Ru) and the effect of $3p$ correlations in the third term (negative); both are of the magnitude 0.5–1%. The estimated baselines are indicated by the shaded bands in Fig. 4.

3.2. Measurements w.r.t. spectator and participant planes

Another comparative measure is $\Delta\gamma$ w.r.t. SP and PP in the same event [44, 45]. Since the magnetic field is more closely connected to SP and the flow to PP, these two $\Delta\gamma$ measurements can uniquely determine the CME and the background. With $\frac{\Delta\gamma_{\mathrm{Bkg}}\{\mathrm{SP}\}}{\Delta\gamma_{\mathrm{Bkg}}\{\mathrm{PP}\}} = \frac{\Delta\gamma_{\mathrm{CME}}\{\mathrm{PP}\}}{\Delta\gamma_{\mathrm{CME}}\{\mathrm{SP}\}} = \langle\cos 2(\Psi_{\mathrm{PP}} - \Psi_{\mathrm{SP}})\rangle \equiv a$, one may obtain the CME fraction as $f_{\mathrm{CME}} \equiv \frac{\Delta\gamma_{\mathrm{CME}}\{\mathrm{PP}\}}{\Delta\gamma\{\mathrm{PP}\}} = \frac{A/a-1}{1/a^2-1}$, where $A = \frac{\Delta\gamma\{\mathrm{SP}\}}{\Delta\gamma\{\mathrm{PP}\}}$.

Figure 5 shows the extracted f_{CME} and $\Delta\gamma_{\mathrm{CME}}$ in Au+Au collisions at $\sqrt{s_{NN}} = 200$ GeV by STAR [46]. The peripheral data are consistent with zero CME with relatively large uncertainties. The mid-central 20–50% data indicate a finite CME signal, with $\sim 2\sigma$ significance. A similar analysis has been performed on 27 GeV data, showing zero CME with present statistics [42].

Similar to isobar collisions, the SP/PP method measures the ratio of two quantities, $A/a = \frac{N\Delta\gamma\{\mathrm{SP}\}/v_2\{\mathrm{SP}\}}{N\Delta\gamma\{\mathrm{PP}\}/v_2\{\mathrm{PP}\}}$. Simpler than the isobar data, only the PP measurements are contaminated by nonflow, $A/a = (1+\epsilon_{\mathrm{nf}})/\left(1+\frac{\epsilon_3/\epsilon_2}{Nv_2\{\mathrm{PP}\}^2}\right)$.

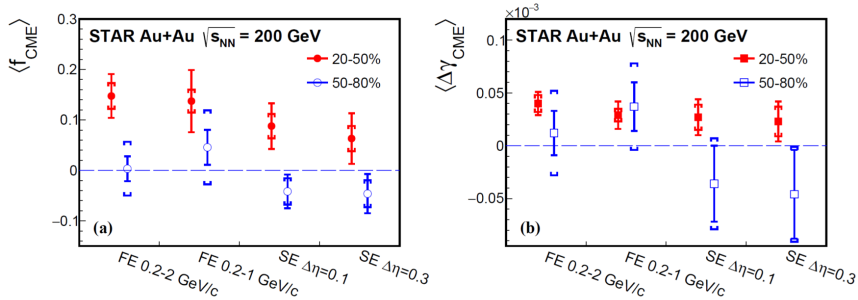

Fig. 5. The extracted CME fraction $f_{\rm CME}$ (left) and CME signal $\Delta\gamma_{\rm CME}$ (right) from $\Delta\gamma$ measurements w.r.t. SP and PP in Au+Au collisions at 200 GeV by STAR [46].

Nonflow in v_2 yields a positive $f_{\rm CME}$ while $3p$ correlations result in a negative $f_{\rm CME}$. There is a good level of cancellation between the two, and the net effect could even be negative [43]. Although model-dependent, it suggests that the measured positive $f_{\rm CME}$ in data might indeed be a hint of CME.

4. Summary and outlook

In summary, measurements of the charge correlator $\Delta\gamma$ and its variants are reviewed. The $\Delta\gamma$ measurements are dominated by backgrounds arising from genuine particle correlations coupled with elliptic flow v_2. Several methods have been devised to eliminate those backgrounds, including event-shape engineering, isobar collisions, and measurements w.r.t. spectator and participant planes. While the first two yield a CME signal consistent with zero with the present statistics, the third indicates a hint of the possible CME in Au+Au collisions with $\sim 2\sigma$ significance. All these methods are subject to nonflow effects, the magnitudes of which are under active investigation.

To outlook, an order of magnitude statistics is anticipated of Au+Au collisions from 2023 and 2025 by STAR. This would present a powerful data sample to either identify the CME or put a stringent upper limit on it.

This work was supported by the U.S. Department of Energy (No. DE-SC0012910) and the China National Natural Science Foundation (Nos. 12035006, 12075085, 12147219).

REFERENCES

[1] D. Kharzeev, R.D. Pisarski, M.H.G. Tytgat, *Phys. Rev. Lett.* **81**, 512 (1998).
[2] D. Kharzeev, L. McLerran, H. Warringa, *Nucl. Phys. A* **803**, 227 (2008).
[3] D.E. Kharzeev, J. Liao, S.A. Voloshin, G. Wang, *Prog. Part. Nucl. Phys.* **88**, 1 (2016).
[4] D. Kharzeev, *Phys. Lett. B* **633**, 260 (2006).
[5] B. Müller, A. Schäfer, *Phys. Rev. D* **98**, 071902 (2018).

[6] V.V. Skokov, A.Yu. Illarionov, V.D. Toneev, *Int. J. Mod. Phys. A* **24**, 5925 (2009).
[7] S.A. Voloshin, *Phys. Rev. C* **70**, 057901 (2004).
[8] N.N. Ajitanand, R.A. Lacey, A. Taranenko, J.M. Alexander, *Phys. Rev.* **83**, 011901 (2011).
[9] A.H. Tang, *Chinese Phys.* **44**, 054101 (2020).
[10] S. Choudhury *et al.*, *Chinese Phys. C* **46**, 014101 (2022).
[11] STAR Coll. (B.I. Abelev *et al.*), *Phys. Rev. Lett.* **103**, 251601 (2009).
[12] STAR Coll. (B.I. Abelev *et al.*), *Phys. Rev. C* **81**, 054908 (2010).
[13] STAR Coll. (L. Adamczyk *et al.*), *Phys. Rev. C* **88**, 064911 (2013).
[14] ALICE Coll. (B.I. Abelev *et al.*), *Phys. Rev. Lett.* **110**, 012301 (2013).
[15] F. Wang, *Phys. Rev. C* **81**, 064902 (2010).
[16] A. Bzdak, V. Koch, J. Liao, *Phys. Rev. C* **81**, 031901 (2010).
[17] S. Schlichting, S. Pratt, *Phys. Rev. C* **83**, 014913 (2011).
[18] J. Zhao, F. Wang, *Prog. Part. Nucl. Phys.* **107**, 200 (2019).
[19] ALICE Coll. (S. Acharya *et al.*), *J. High Energy Phys.* **2020**, 160 (2020).
[20] CMS Coll. (V. Khachatryan *et al.*), *Phys. Rev. Lett.* **118**, 122301 (2017).
[21] STAR Coll. (J. Adam *et al.*), *Phys. Lett. B* **798**, 134975 (2019).
[22] R. Belmont, J.L. Nagle, *Phys. Rev. C* **96**, 024901 (2017).
[23] STAR Coll. (J. Adam *et al.*), *Phys. Rev. C* **106**, 034908 (2022).
[24] W. Li, G. Wang, *Annu. Rev. Nucl. Part. Sci.* **70**, 293 (2020).
[25] STAR Coll. (L. Adamczyk *et al.*), *Phys. Rev. Lett.* **113**, 052302 (2014).
[26] A. Bzdak, V. Koch, J. Liao, *Lect. Notes Phys.* **871**, 503 (2013).
[27] CMS Coll. (A.M. Sirunyan *et al.*), *Phys. Rev. C* **97**, 044912 (2018).
[28] STAR Coll. (L. Adamczyk *et al.*), *Phys. Rev. C* **89**, 044908 (2014).
[29] F. Wen, J. Bryon, L. Wen, G. Wang, *Chinese Phys. C* **42**, 014001 (2018).
[30] F. Wang, J. Zhao, *Phys. Rev. C* **95**, 051901 (2017).
[31] ALICE Coll. (S. Acharya *et al.*), *Phys. Lett. B* **777**, 151 (2018).
[32] J. Schukraft, A. Timmins, S.A. Voloshin, *Phys. Lett. B* **719**, 394 (2013).
[33] S.A. Voloshin, *Phys. Rev. Lett.* **105**, 172301 (2010).
[34] V. Koch *et al.*, *Chinese Phys. C* **41**, 072001 (2017).
[35] W.-T. Deng, X.-G. Huang, G.-L. Ma, G. Wang, *Phys. Rev. C* **94**, 041901 (2016).
[36] STAR Coll. (M.S. Abdallah *et al.*), *Phys. Rev. C* **105**, 014901(R) (2022).
[37] Y. Feng, Y. Lin, J. Zhao, F. Wang, *Phys. Lett. B* **820**, 136549 (2021).
[38] H.-j. Xu *et al.*, *Phys. Rev. Lett.* **121**, 022301 (2018).
[39] H.-j. Xu *et al.*, *Phys. Lett. B* **819**, 136453 (2021).
[40] H. Li *et al.*, *Phys. Rev. C* **98**, 054907 (2018).
[41] STAR Coll. (J. Adam *et al.*), *Nucl. Sci. Tech.* **32**, 48 (2021).
[42] STAR Coll. (P. Tribedy), *Acta Phys. Pol. B Proc. Suppl.* **16**, 1-A6 (2023), this issue.
[43] Y. Feng *et al.*, *Phys. Rev. C* **105**, 024913 (2022).
[44] H.-J. Xu *et al.*, *Chinese Phys. C* **42**, 084103 (2018).
[45] S.A. Voloshin, *Phys. Rev. C* **98**, 054911 (2018).
[46] STAR Coll. (M.S. Abdallah *et al.*), *Phys. Rev. Lett.* **128**, 092301 (2022).